Available online at www.sciencedirect.com

SciVerse ScienceDirect

Ceramics International 38 (2012) 4305–4312

CERAMICS INTERNATIONAL

www.elsevier.com/locate/ceramint

Effects of Fe–Ni alloy nanoparticles on the mechanical properties and microstructures of Al_2O_3/Fe–Ni nanocomposites prepared by rapid sintering

Young-In Lee [a], Jun-Tae Lee [a,b], Yong-Ho Choa [a,*]

[a] Department of Fine Chemical Engineering, Hanyang University, Ansan 426-791, Republic of Korea
[b] Material Testing Center, Korea Testing Laboratory, Ansan 426-791, Republic of Korea

Received 24 January 2012; received in revised form 2 February 2012; accepted 2 February 2012
Available online 19 February 2012

Abstract

A high frequency induction heated sintering (HFIHS) process was applied to fabricate dense Al_2O_3 reinforced with Fe–Ni magnetic metal dispersion particles. The process is based on the reduction of metal oxide particles immediately prior to sintering. The synthesized Al_2O_3/Fe–Ni nanocomposite powders are formed directly from the selective reduction of metal oxide powders, including NiO and Fe_2O_3. A dense Al_2O_3/Fe–Ni nanocomposite was fabricated using the HFIHS method with an extremely high heating rate of 2000 °C/min. The phase identification of nanocomposite powders and sintered specimens was determined by X-ray diffraction. Three-point bending tests and Vickers hardness experiments were performed to investigate the mechanical properties of the Al_2O_3/Fe–Ni nanocomposites and the relationship between microstructure and mechanical properties was investigated using TEM and SEM supported with EDX.

Keywords: B. Nanocomposite; C. Mechanical properties; High frequency induction heated sintering (HFIHS); Fe–Ni dispersion particle; $FeAl_2O_3$ spinel; Microstructure

1. Introduction

Alumina (Al_2O_3) is one of the most widely used ceramic materials for structural applications because it possesses favorable physical and chemical properties, such as high strength, high hardness, high elastic modulus and excellent resistance to thermal and chemical environments [1,2]. However, the relatively low fracture toughness of monolithic alumina is a limiting factor for engineering applications in severe conditions. The brittle ceramics can be toughened by the incorporation of ductile metallic phase attributed to a crack bridging mechanism [3,4] and thus much attention has been focused on the development of Al_2O_3/metal nanocomposites for decades. Various secondary metallic nanoparticles including Cu [5], Fe [6,7], Ni [8,9], Co [10], Fe–Ni [11–13], Fe–Cr [14], and Zn–Ni [15,16] were dispersed into Al_2O_3 materials to enhance mechanical properties and corrosion resistant and to create catalytic and magnetic properties.

The grain refinement for nanocrystalline and reaction phase inhibition between ceramic matrix and metal dispersant are important considerations on the sintering of the ceramic/metal nanocomposites for outstanding mechanical properties. If the sintering is carried out using traditional methods such as resistance heating without external pressure, the nanocomposites have the microstructural coarsening and reaction phases were easily formed because high temperature and long time for full densification of the specimen were required. In the past, many researchers have postulated that a rapid sintering method may maximize densification with minimum microstructural (mainly grain) coarsening and forming reaction phases [17–19]. In this scenario, a rapid heating rate is applied to a powder compact such that the sample spends little time in the low temperature regime, where non-densifying mechanisms such as surface diffusion are active, and proceeds quickly to higher temperatures where densifying mechanisms, such as grain boundary or volume diffusion, are dominant. An external pressure is also essential to fabricate a sintered body with a full relative density during a shorter sintering time because the thermal diffusion and plastic flow caused by the high pressure are able to enhance sinterability.

* Corresponding author.
E-mail address: choa15@hanyang.ac.kr (Y.-H. Choa).

0272-8842/$36.00
doi:10.1016/j.ceramint.2012.02.011

In this regard, high frequency induction heated sintering (HFIHS) method that utilizes a high-frequency magnetic field generated by applying a high-frequency electric current through a coil which encompasses the materials is a type of a solid compression sintering process combined with high pressure (hot pressing) and rapid heating rate (rapid sintering) [20–23]. Therefore the method is suitable to obtain fully densified Al_2O_3/metal nanocomposites with the nanocrystalline structure and the minimized reaction phases. In this study, Al_2O_3/Fe–Ni nanocomposite powder was synthesized from as-prepared Al_2O_3/($NiO{\cdot}Fe_2O_3$) by selective reduction process and sintered using the HFIHS method to fabricate the highly densified and strengthened Al_2O_3/Fe–Ni nanocomposite that has potential applications as structural/magnetic materials. Furthermore, this work is also aimed to investigate the optimized sintering conditions for HFIF processing and the effect of Fe–Ni dispersion particles and $FeAl_2O_3$ spinel phase contents on the mechanical properties including fracture strength, fracture toughness, and hardness of Al_2O_3/Fe–Ni nanocomposites.

2. Experimental

2.1. Powder synthesis procedure

Starting materials were prepared from the following: α-Al_2O_3 powder (AKP-53, Sumitomo Chem. Co., Japan 99.99%, average particle size 0.2 μm) as a matrix material, Fe-nitrate ($Fe(NO_3)_2{\cdot}9H_2O$, purity 99.9%) and Ni-nitrate ($Ni(NO_3)_2{\cdot}6H_2O$, $6H_2O$, purity 99.9%) as a source of Fe and Ni, respectively. The ratio was aimed at final compositions of Al_2O_3/10 wt%Fe–Ni. The Fe- and Ni-nitrate were dissolved in ethanol (purity 99.5%) using a hot plate at 40 °C for 30 min, then wet milled with Al_2O_3 powder in alcohol using 200 ml of high-purity Al_2O_3 balls (diameter: 5 mm) in a polyethylene container for 24 h. The slurries were dried and calcined using an evaporator at 40 °C and an electric furnace at 400 °C for 2 h in air, respectively. After the calcination process, wet milling and drying were repeated with the same conditions. To remove the hard, agglomerated particles, dry milling was performed using high-purity Al_2O_3 balls (diameter: 10 mm) in a polyethylene container for 24 h. The ball-milled powders ($Al_2O_3(NiO{\cdot}Fe_2O_3)$) were reduced by increasing the temperature up to 700 °C for 1 h in a hydrogen atmosphere to synthesize Al_2O_3/Fe–Ni nanocomposite powders. The reduction behavior of the $Al_2O_3(NiO{\cdot}Fe_2O_3)$ powder mixture was analyzed using an *in situ* measuring method [4,8], in which the hygrometry system for measuring the relative humidity of the outlet gas was equipped with a thermogravimetry (TG) system to monitor the progress of the reduction reaction. Thermogravimetry analysis was conducted by increasing the temperature up to 700 °C with a heating rate of 10 °C/min for 1 h in a hydrogen atmosphere (dew point −76 °C, flow rate 0.4 l/min).

2.2. Fabrication of dense Al_2O_3/Fe–Ni nanocomposite

The calcined powders were heated to 700 °C for 1 h in hydrogen to reduce the metal oxides, and the Al_2O_3/10 wt% Fe–Ni nanocomposite (denoted by AFN10 nanocomposite) powders were selectively reduced and sintered using the HFIHS process to fabricate dense AFN10 nanocomposites. The reduced powders were placed in a graphite mold (outside diameter, 45 mm; inside diameter, 20 mm; height, 40 mm) and introduced into the system. The system was first evacuated and sintered at 1000–1400 °C for 5 min with a heating rate of 2000 °C/min. During the sintering procedure, a uniaxial pressure of 50 MPa was applied and maintained until densification was attained. Temperatures were measured using a pyrometer focused on a graphite mold surface. At the end of the process, the samples were cooled to room temperature.

2.3. Evaluation of mechanical properties

The densities of the sintered specimens were measured using the Archimedes method with toluene as the media. For bending experiments, sintered specimens were ground and then cut using an automatic saw resulting in samples with dimensions 4 mm × 3 mm × 37 mm. The specimens were then polished to 0.2 μm and chamfered to eliminate large surface flaws resulting from the cutting process. The fracture strengths of the sintered samples were measured using three-point bending with a cross-head speed of 0.5 mm/min. Vickers hardness and fracture toughness were measured by performing indentations at a load of 10 kg and a dwell time 15 s. The fracture toughness, K_{IC}, was calculated using the following empirical equation for a median crack [24];

$$\frac{K_{IC}}{H_V a^{1/2}} = 0.203\left(\frac{c}{a}\right)^{-3/2} \quad (1)$$

where c and a are the lengths of the median crack and half of the diagonal of the indentation, respectively. The indentation with a load of 10 kg was performed on the polished surface of the specimen. X-ray diffraction was used for phase identification. The microstructures of the nanocomposites were studied by TEM and SEM assisted by EDX.

3. Results and discussion

3.1. Simultaneous reduction and synthesis of Al_2O_3/Fe–Ni nanocomposite powder

The X-ray diffraction patterns shown in Fig. 1(a) clearly show that the initial powder mixture, which consists of Al_2O_3, Fe-nitrate, and Ni-nitrate, turned into Al_2O_3, NiO, and Fe_2O_3 phases after the calcinations process (Fig. 1(b)). Thermogravimetric analyses was performed for the Al_2O_3/($NiO{\cdot}Fe_2O_3$) powder mixture prepared by ball milling followed by calcinations to investigate the reduction behavior of Fe and Ni oxides. Fig. 2 shows the variation of weight loss during heating to 700 °C with a heating rate of 10 °C/min for 1 h in a hydrogen atmosphere. The weight loss gradually decreased with increasing temperature and then decreased abruptly at 300 °C, finally reaching full reduction state at 700 °C. This information indicates that the hydrogen reduction reaction of the Al_2O_3/($NiO{\cdot}Fe_2O_3$) powder mixture started at 300 °C, then finished at 700 °C. Based on the results of the hygrometry

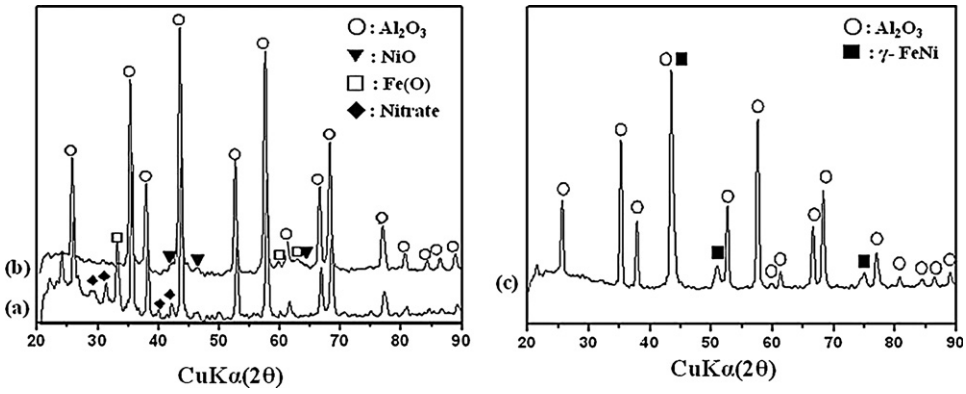

Fig. 1. XRD patterns of (a) the initial powder, (b) after calcination, and (c) after H_2 reduction at 700 °C for 1 h.

analysis, the hydrogen reduction of $Al_2O_3/(NiO{\cdot}Fe_2O_3)$ powder was performed at 700 °C with a heating rate 10 °C/min for 1 h. As shown in Fig. 1(c), the X-ray diffraction patterns showed only reflections from Al_2O_3 and γ-FeNi for the reduced sample indicating that homogeneously mixed Fe- and Ni-oxides were reduced and occurred during *in situ* alloying of Fe–Ni metal particle.

Fig. 3 shows TEM micrographs of the AFN10 nanocomposite powder reduced in hydrogen at 700 °C for 1 h. Arrows indicate homogeneously dispersed γ-Fe–Ni particles having an average particle diameter of 20 nm on Al_2O_3 matrix with an average particle size of 150 nm. As shown in the X-ray diffraction and TEM results, the chemical route process using metal-nitrates was suitable for the fabrication of homogeneously dispersed ceramic/metal nanocomposite powder.

3.2. Microstructure and sinterability

As we previously reported rapid sintering processes have various advantages compared with the HP process [20–23]. Therefore, it is expected that the HFIHS process when applying an extremely rapid heating rate is a feasible approach to address the problem caused by the $FeAl_2O_3$ reaction phase, because rapid sintering provides a lower sintering temperature and shorter heating time than HP process. From this point of view, an extremely high heating rate of 2000 °C/min was applied to fabricate dense AFN10 nanocomposites by the HFIHS method.

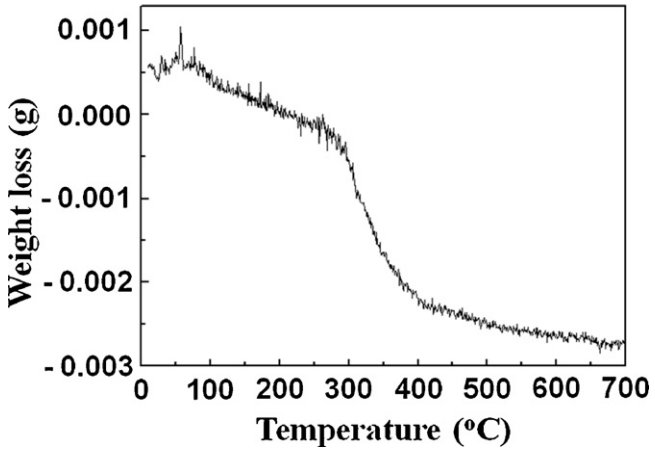

Fig. 2. Variation of weight loss during TG analysis for calcined powder mixture ($Al_2O_3/NiO{\cdot}Fe_2O_3$) with a heating rate of 10 °C/min for 1 h in H_2 atmosphere.

Fig. 4 shows the X-ray diffraction profiles of the AFN10 nanocomposites: (a) sintered by the HFIHS method at 1100 °C, and (b) 1400 °C for 5 min in vacuum with heating rate of 2000 °C/min. Even though the $FeAl_2O_4$ spinel phase was also observed in the XRD analysis for the HFIHS processed specimens, the relative peak intensity of the $FeAl_2O_4$ spinel phase compared to the Fe–Ni alloy phase, calculated in Table 1, interestingly shows that although rapid sintering with an extremely high heating rate was performed, the $FeAl_2O_4$ spinel phase was formed. However, the amount of $FeAl_2O_4$ was minimized by controlling the sintering temperature. Spinel $FeAl_2O_4$ showed a minimum value at 1100 °C, then increased with increasing sintering temperature. The reduced formation of the $FeAl_2O_4$ spinel phase was caused by a shorter holding time and lower sintering temperature compared to the HP process due to the extremely rapid heating rate of the HFIHS process.

As shown in Figs. 5 and 6, SEM images of the fracture surface for the Al_2O_3 monolith (Fig. 5) and AFN10 nanocomposite (Fig. 6) fabricated by the HFIHS method clearly show that the average grain size of the Al_2O_3 monolith and AFN nanocomposite are submicron size up to 1100 °C, then, they abruptly increase at temperature greater than 1200 °C. While the microstructural changes of both the Al_2O_3 monolith and AFN10 nanocomposite have an increasing tendency with increasing sintering temperature, the grain size of the AFN10 nanocomposite was slightly smaller than the Al_2O_3 monolith at the same temperatures. For the AFN10 nanocomposites, the refinement of the Al_2O_3 matrix grain size was due to the retardation of alumina grain growth resulted from homogeneously dispersed Fe–Ni metal particles. Dispersion particles, in general, inhibit grain boundary migration of the matrix. However, for finer dispersion particles, the matrix grain boundary can pass through the dispersion particles, which were absorbed into the matrix grains. Alternatively, the larger dispersion particles remain at the grain boundaries without being absorbed into the matrix grain, because the grain boundary cannot pass through the larger dispersion particles [25,26]. The Fe–Ni dispersion particle size was determined

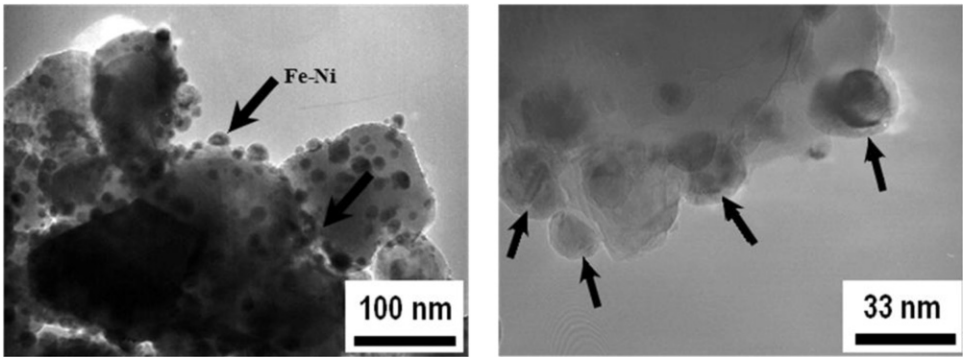

Fig. 3. TEM images of AFN10 nanocomposite powder reduced at 700 °C for 1 h in H_2 atmosphere (arrows indicate γ-FeNi dispersion particle).

using a linear intercept method as 80, 100, 170, and 300 nm, for the AFN10 nanocomposite with temperatures of 1000 °C, 1100 °C, 1200 °C, and 1300 °C, respectively. This increasing tendency of Fe–Ni dispersion particles with increasing sintering temperature was due to the migration of the metal phase at the initial stages of sintering and coalescence of the metal phase accompanied by grain growth of alumina matrix at the final stages. The grain size of the AFN10 nanocomposite was finer than that of Al_2O_3 monolith based on the inhabitation of the grain growth by the second dispersion phase.

The microstructural changes observed for both the Al_2O_3 monolith and AFN10 nanocomposite were congruent with the density and Vickers hardness shown in Fig. 7(a) and (b), respectively. The density of the AFN10 nanocomposite shows a maximum value at 1200 °C and then decreases with increasing sintering temperature. The decrease in densification was due to the formation of $FeAl_2O_4$, which has a lower theoretical density. One explanation for the retardation of densification could be the difficulty distributing Fe–Ni particulates, which decreases the sintering rate by inducing a tensile mean stress that develops from differential shrinkage characteristics between Al_2O_3 matrix and Fe–Ni dispersion [25]. In addition, grain boundary diffusivity is expected to decrease with increasing Fe–Ni addition [26], for which the grain boundary diffusion is a predominant mechanism of matter transformation [27]. When the Fe–Ni particulate is located at the grain boundaries, the grain boundary diffusion path becomes longer with respect to the diameter of the Fe–Ni particulate, and the diffusion of atoms/vacancies along the interface between the Al_2O_3 grain and Fe–Ni particle should be slower. Therefore, the observed retardation of densification is due to the decrease in the grain boundary diffusivity which results from the Fe–Ni dispersion.

Even though the densification was depressed by the Fe–Ni dispersion phase, all samples were highly densified due to the increased sinterability caused by the rapid heating rate. Lee and coworkers reported that the sintering temperature of an Al_2O_3/10 wt%Fe–Ni nanocomposite fabricated by the HP process was 1450 °C which was greater than the HFIHS method [28]. In the HFIHS method, a rapid heating rate was applied to a powder compact such that the sample quickly avoided the low temperature regime, where nondensifying mechanisms such as surface diffusion are active, and proceeded directly to high temperatures where densifying mechanisms, such as grain boundary or volume diffusion dominate. Since grain growth occurs in both regimes, the use of rapid heating rates can greatly improve the final sintered density for a given grain size. For the Al_2O_3 material, the enthalpy of the lattice diffusion and surface diffusion was 578 and 234–280 kJ/mol, respectively. Therefore, a rapid heating rate promotes the lattice diffusion and/or grain boundary diffusion, which are main densification mechanisms in the high temperature regime, rather than surface diffusion as a coarsening mechanism. As a result, the faster heating rate of the HFIHS process enhanced the densification.

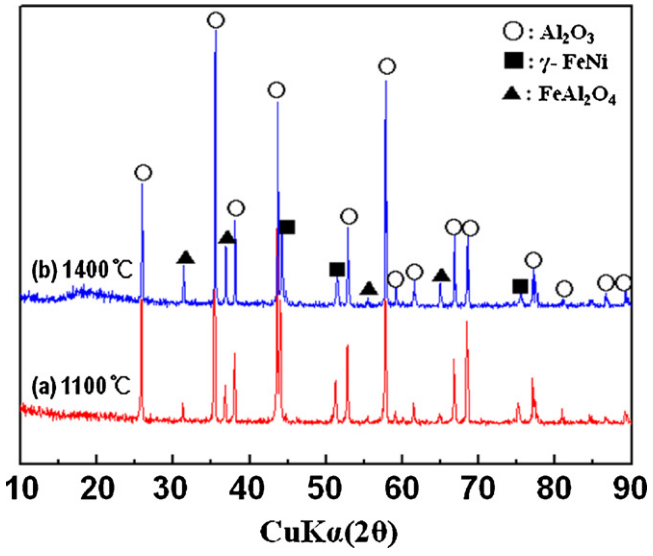

Fig. 4. XRD diffraction patterns of the AFN10 nanocomposites; (a) sintered by the HFIHS method at 1100 °C for 5 min, and (b) 1400 °C for 5 min in a vacuum with a heating rate of 2000 °C/min.

Table 1
The peak intensity ratio of the $FeAl_2O_4$ phase with respect to the Fe–Ni and $FeAl_2O_4$ phase.

Temperature (°C)	$I_{FeAl_2O_4}/(I_{FeNi} + I_{FeAl_2O_4})$
1100	0.224
1200	0.286
1300	0.411
1400	0.418

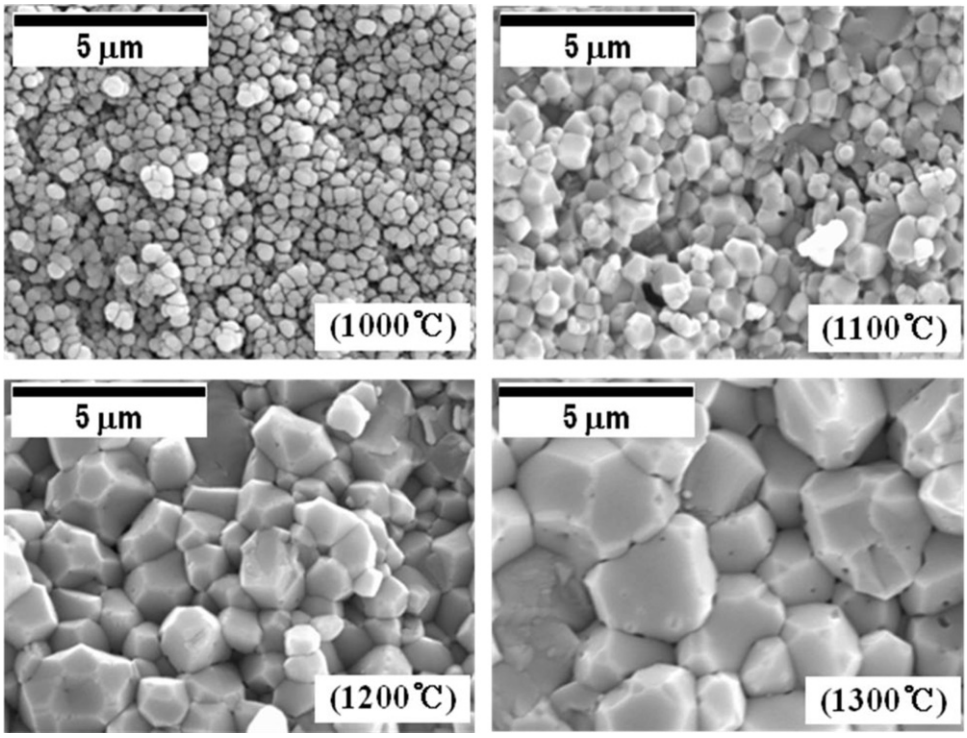

Fig. 5. SEM micrographs of the fracture surface for the Al_2O_3 monolith fabricated by the HFIHS method with a heating rate of 2000 °C/min.

3.3. Fracture strength and toughness

The fracture strength and toughness were enhanced by the HFIHS process compared to the HP process. Previous literature reported that the maximum fracture strength and toughness of an AFN10 nanocomposite fabricated by the HP process were 389 MPa and 3.87 MPa $m^{1/2}$, respectively [23]. In addition, Zhang et al. reported Al_2O_3/FeNi composites fabricated by hot pressing at 1400 °C and the sample indicated the fracture strength of 600 MPa and the fracture toughness of

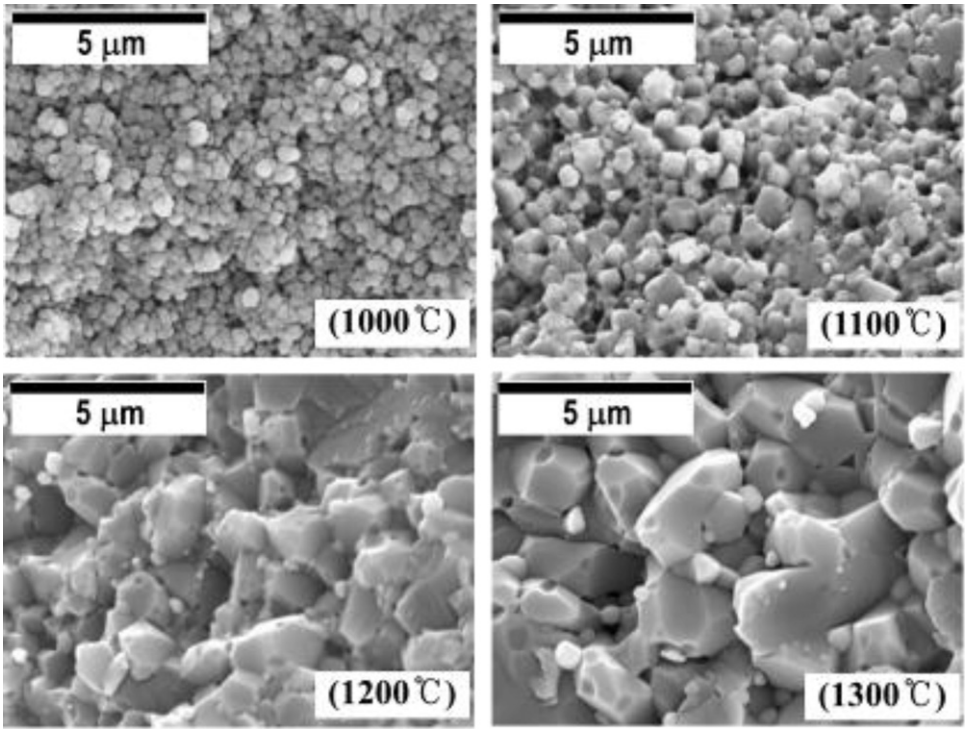

Fig. 6. SEM micrographs of the fracture surface for AFN10 nanocomposite fabricated by HFIHS method with a heating rate of 2000 °C/min.

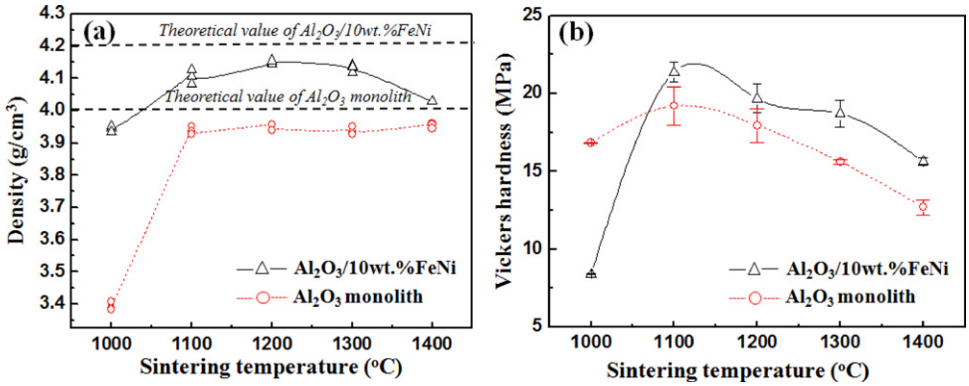

Fig. 7. (a) Densities of the Al_2O_3 monolith and AFN10 nanocomposite and (b) Vickers hardness as a function of sintering temperature.

5.0 MPa $m^{1/2}$ at 10 wt% FeNi content, respectively [13]. The maximum strength and fracture toughness of the AFN10 nanocomposite fabricated by the HFIHS method at 1200 °C were 800 MPa and 5.1 MPa $m^{1/2}$, respectively. Fig. 8 shows the fracture strength and toughness for both the Al_2O_3 monolith and AFN10 nanocomposite sintered by the HFIHS method as a function of the sintering temperature. The fracture strength for the monolithic Al_2O_3 showed a maximum value at 1100 °C, then, decreased with increasing temperature. Alternatively, the maximum fracture strength for the AFN10 nanocomposite was obtained at 1200 °C, and then decreased at temperatures greater than 1200 °C. As shown in Figs. 5 and 6, there was no significant change in the grain size of the AFN10 nanocomposite compared with monolithic Al_2O_3 based on the SEM observations of the fracture surface for both the Al_2O_3 monolith and AFN10 nanocomposite. Thus, the refinement of Al_2O_3 matrix grain size as a critical flaw size for fracture does not account for the significant change in fracture strength as a function of temperature [29]. The variation of fracture strength can be explained in terms of fracture toughness and the formation of a $FeAl_2O_4$ spinel phase. Generally, an increase in fracture toughness for monolithic Al_2O_3 can be achieved by a grain bridging mechanism with increasing the grain size [24]. Thus, as fracture strength of the AFN10 nanocomposite was congruent with that of fracture toughness, the increase in fracture toughness up to 1200 °C was caused by the yielding/bridging mechanism. We also expected that the maximum fracture strength of AFN10 nanocomposite might be attained at 1200 °C because this temperature produced the highest density, as shown in Fig. 7. Additionally, the decreasing tendency of the fracture strength at the temperatures greater than 1200 °C should be discussed in terms of the formation of the brittle $FeAl_2O_3$ spinel phase for the AFN10 nanocomposite. Considering the formation of the $FeAl_2O_3$ spinel phase, there was an insignificant change up to 1200 °C, then a sudden increase at the temperatures greater than 1200 °C, and the fracture toughness also had a maximum value (5.1 MPa $m^{1/2}$) at 1200 °C and abruptly decreased. This result indicates that the formation of a brittle spinel phase was responsible for the decreasing fracture toughness above 1200 °C. These results indicate that the increasing fracture strength up to 1200 °C was due to the increase in fracture toughness caused by a yielding/bridging mechanism due to the Fe–Ni metal dispersion phase. Additionally, the decreasing tendency over 1200 °C was caused by the formation of a brittle $FeAl_2O_3$ spinel phase.

3.4. Microstructure and yielding/bridging

As previously discussed, the mechanism of improvement for the fracture toughness for the AFN nanocomposite system is best investigated in terms of yielding/bridging by dispersion particulates [30]. Fig. 9 shows the crack propagation introduced by indentation and crack resistance by yielding and bridging of the AFN10 nanocomposite. EDX line analysis was performed

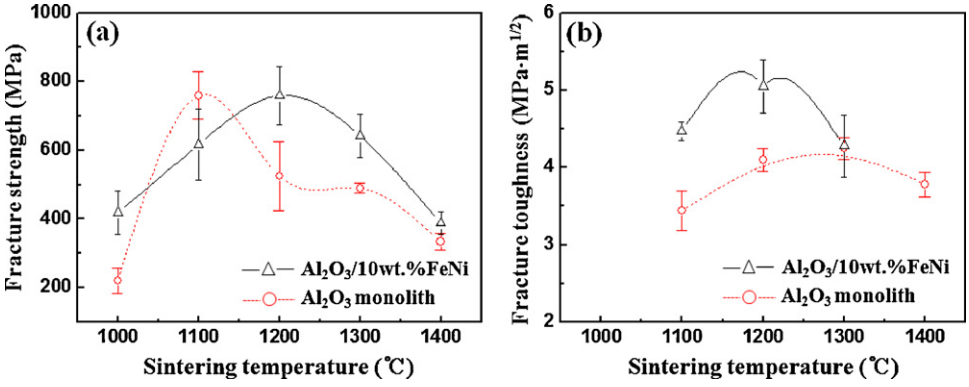

Fig. 8. (a) Fracture strength and (b) fracture toughness of monolithic Al_2O_3 and AFN10 nanocomposite as a function of sintering temperature.

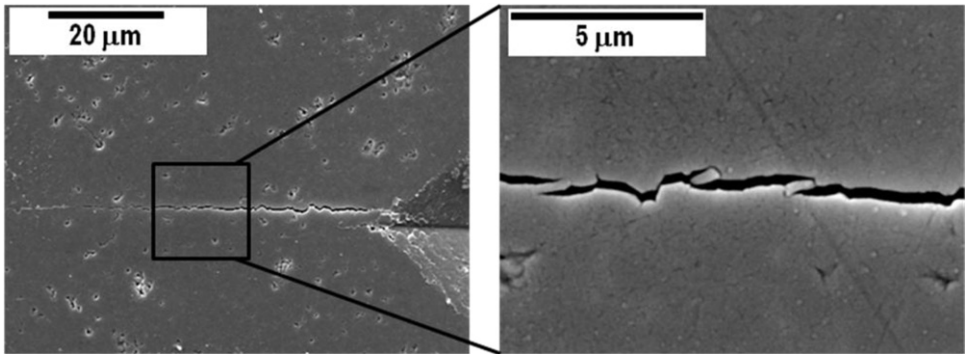

Fig. 9. SEM micrographs of crack introduced by indentation for the AFN10 nanocomposite.

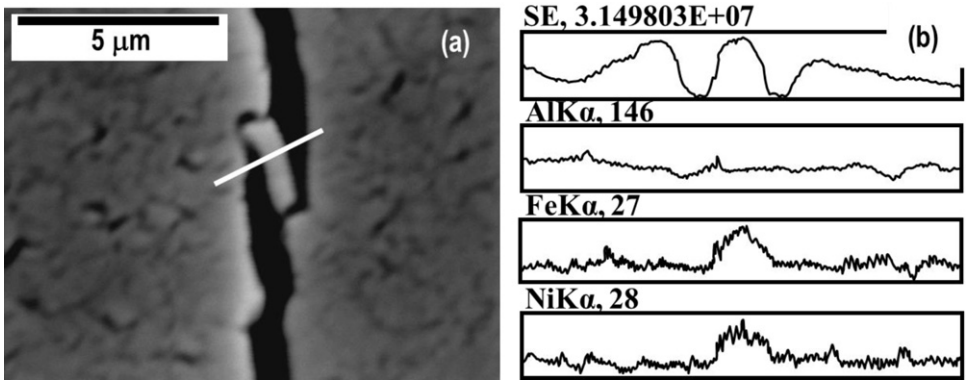

Fig. 10. (a) SEM image and (b) EDX line analysis profile of bridged Fe–Ni dispersion particles.

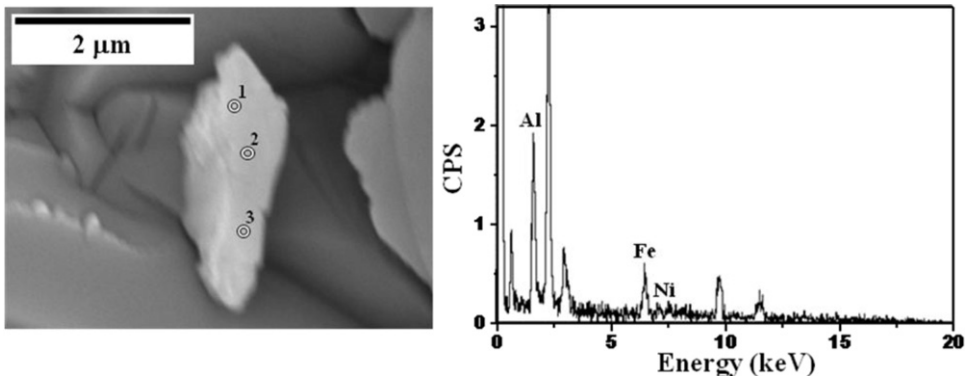

Fig. 11. SEM image and EDX point analysis profile of $FeAl_2O_4$ spinel particles.

to determine which phase was responsible for the yielding/bridging mechanism among the alumina, spinel phase, and metal particle. As shown in Fig. 10, the line analysis results revealed that yielding/bridging was caused by the Fe–Ni particles. Because the EDX analysis included Fe and Ni, the bridging was due to the Fe–Ni metal particle and not $FeAl_2O_4$ spinel phase. Thus, the Fe–Ni metal phase primarily affected the fracture toughness.

Point analyses were performed by EDX to investigate the morphology and composition of the $FeAl_2O_4$ spinel and Fe–Ni metal phase for AFN10 sintered at 1300 °C that had a well-developed $FeAl_2O_4$ spinel phase. As shown in Fig. 11, the EDX point analysis results of the particles that appeared to fail by brittle fracture indicates that it was a $FeAl_2O_4$ spinel phase, because only Al and Fe peaks were observed. As a result, the brittle/weak $FeAl_2O_4$ spinel particle was not effective for toughening, however the Fe–Ni particle caused a yielding/bridging effect.

4. Conclusion

An Al_2O_3/Fe–Ni nanosized metal dispersion nanocomposite powder was successfully fabricated by simultaneous reduction and synthesis using a chemical route process. The HFIHS method as rapid sintering method with external high pressure was applied to sinter the nanocomposite powder. This process

avoids the problems associated with hot-pressing. Enhanced strength and fracture toughness were achieved due to 10 wt% Fe–Ni and were attributed to crack bridging/yielding rather than refinement of the Al_2O_3 matrix microstructure. Enhanced fracture strength and toughness resulted from the HFIHS process compared with the HP process. The maximum strength and fracture toughness of the Al_2O_3/10 wt%Fe–Ni nanocomposite sintered at 1200 °C were 800 MPa and 5.1 MPa $m^{1/2}$, respectively. Alternatively, sintering at higher temperatures leads to a decrease in strength and fracture toughness due to the formation of a brittle $FeAl_2O_4$ spinel phase. The existence of a $FeAl_2O_4$ spinel and Fe–Ni metal dispersion particles were confirmed by EDX analysis. Yielding/bridging, which affected the fracture toughness, is caused by a Fe–Ni metal phase.

Acknowledgments

This work was supported by the Human Resources Development of the Korea Institute of Energy Technology Evaluation and Planning (KETEP) grant funded by the Ministry of Knowledge Economy, Republic of Korea (20104010100620).

References

[1] R. Fan, B. Liu, J. Zhang, J. Bi, Y. Yin, Kinetic evaluation of combustion synthesis $3TiO_2 + 7Al \rightarrow 3TiAl + 2Al_2O_3$ using non-isothermal DSC method, Mater. Chem. Phys. 91 (2005) 140–145.

[2] G.P. Kelkar, A.H. Carim, Phase equilibria in the Ti–AI–O system at 945 °C and analysis of Ti/Al_2O_3 reactions, J. Am. Ceram. Soc. 78 (1995) 572–576.

[3] T.J. Marrow, G.A.D. Briggs, S.G. Roberts, In situ scanning acoustic microscopy of crack bridging in alumina, J. Eur. Ceram. Soc. 14 (1994) 111–116.

[4] W.G. Fahrenholtz, D.T. Ellerby, R.E. Loehman, Al_2O_3–Ni composites with high strength and fracture toughness, J. Am. Ceram. Soc. 83 (2000) 1279–1280.

[5] K.H. Min, S.T. Oh, Y.D. Kim, I.H. Moon, Processing and fracture toughness of nano-sized Cu-dispersed Al_2O_3 composites, J. Alloys Compd. 352 (2003) 163–167.

[6] J.G. Santanach, C. Estournes, A. Weibel, A. Peigney, G. Chevallier, Ch. Laurent, Spark plasma sintering as a reactive sintering tool for the preparation of surface-tailored Fe–$FeAl_2O_4$–Al_2O_3 nanocomposites, Scripta Mater. 60 (2009) 195–198.

[7] K.R. Ravi, A. Murugesan, V. Udhayabanu, R. Subramanian, B.S. Murty, Microstructure and mechanical property of Fe–Al_2O_3 nanocomposites synthesized by reactive milling followed by spark plasma sintering, Mater. Sci. Forum 710 (2012) 291–296.

[8] Q. Feng, T. Li, H. Teng, X. Zhang, Y. Zhang, C. Liu, J. Jin, Investigation on the corrosion and oxidation resistance of Ni–Al_2O_3 nano-composite coatings prepared by sediment co-deposition, Surf. Coat. Technol. 202 (2008) 4137–4144.

[9] T. Isobea, K. Daimona, T. Satoa, T. Matsubaraa, Y. Hikichia, T. Otab, Spark plasma sintering technique for reaction sintering of Al_2O_3/Ni nanocomposite and its mechanical properties, Ceram. Int. 34 (2008) 213–217.

[10] E. Menendez, G. Salazar-Alvarez, A.P. Zhilyaev, S. Surinach, M.D. Baro, J. Nogues, J. Sort, Cold consolidation of metal–ceramic nanocomposite powders with large ceramic fractions, Adv. Funct. Mater. 18 (2008) 3293–3298.

[11] L. Wang, D. Li, M. Koike, S. Koso, Y. Nakagawa, Y. Xu, K. Tomishige, Catalytic performance and characterization of Ni–Fe catalysts for the steam reforming of tar from biomass pyrolysis to synthesis gas, Appl. Catal. A 392 (2011) 248–255.

[12] S. Vitta, V. Sinha, D. Bahadur, Magnetic properties of $(Fe)_{1-x}$–$(Al_2O_3)_x$ and $(Fe_{50}Ni_{50})_{1-x}$–$(Al_2O_3)_x$ nanocomposite magnetic media synthesized using gel like Al_2O_3 matrix, J. Alloys Compd. 482 (2009) 155–159.

[13] X.Y. Qin, R. Cao, H.Q. Li, Fabrication and mechanical properties of ultrafine grained-Ni–20Fe/Al_2O_3 composites, Ceram. Int. 32 (2006) 575–581.

[14] J.G. Santanach, C. Estournes, A. Weibel, A. Peigney, G. Chevallier, Ch. Laurent, Mechanical and tribological properties of Fe/Cr–$FeAl_2O_4$–Al_2O_3 nano/micro hybrid composites prepared by spark plasma sintering, Scripta Mater. 64 (2011) 777–780.

[15] H.Y. Zheng, M.Z. An, Electrodeposition of Zn–Ni–Al_2O_3 nanocomposite coatings under ultrasound conditions, J. Alloys Compd. 459 (2008) 548–552.

[16] H. Zheng, M. An, J. Lu, Corrosion behavior of Zn–Ni–Al_2O_3 composite coating, Rare Met. 25 (2006) 174–178.

[17] W. Li, L. Gao, Rapid sintering of nanocrystalline ZrO_2(3Y) by spark plasma sintering, J. Eur. Ceram. Soc. 20 (2000) 2441–2445.

[18] J. Zhang, R. Tu, T. Goto, Spark plasma sintering of Al_2O_3–cBN composites facilitated by Ni nanoparticle precipitation on cBN powder by rotary chemical vapor deposition, J. Eur. Ceram. Soc. 31 (2011) 2083–2087.

[19] M. Gupta, W.L.E. Wong, Enhancing overall mechanical performance of metallic materials using two-directional microwave assisted rapid sintering, Scripta Mater. 52 (2005) 479–483.

[20] S.W. Kim, K.A.R. Khalil, High-frequency induction heat sintering of mechanically alloyed alumina–yttria-stabilized zirconia nano-bioceramics, J. Am. Ceram. Soc. 89 (2006) 1280–1285.

[21] I.J. Shon, I.K. Jeong, J.H. Park, B.R. Kim, K.T. Lee, Effect of Fe_2O_3 addition on consolidation and properties of 8 mol% yttria-stabilized zirconia by high-frequency induction heated sintering (HFIHS), Ceram. Int. 35 (2009) 363–368.

[22] H.C. Kim, I.J. Shon, Z.A. Munir, Rapid sintering of ultra-fine WC–10 wt% Co by high-frequency induction heating, J. Mater. Sci. 40 (2005) 2849–2854.

[23] I.J. Shon, T.W. Kim, J.M. Do, J.K. Yoon, S.W. Park, I.Y. Ko, Mechanical synthesis and rapid consolidation of a nanocrystalline $3.3Fe_{0.6}Cr_{0.3}Al_{0.1}$–$Al_2O_3$ composite by high frequency induction heating, J. Alloys Compd. 509 (2011) L7–L10.

[24] Y.H. Choa, A. Nakahira, K. Niihara, Microstructure and mechanical properties of SiC-platelet reinforced Al_2O_3/SiC-particle hybrid composites, J. Mater. Sci. 35 (2000) 3143–3149.

[25] N. Bamba, Y.H. Choa, T. Sekino, K. Niihara, Microstructure and mechanical properties of yttria stabilized zirconia/silicon carbide nanocomposites, J. Eur. Ceram. Soc. 18 (1998) 693–699.

[26] A. Niihara, K. Niihara, Sintering behaviors and consolidation process for Al_2O_3/SiC nanocomposites, J. Ceram. Soc. Jpn. 100 (1992) 448–453.

[27] J.E. Burke, Role of grain boundaries in sintering, J. Am. Ceram. Soc. 40 (1957) 80–85.

[28] H.J. Lee, Y.K. Jeong, S.T. Oh, J.S. Lee, T. Sekino, Fabrication of Al_2O_3/Fe–Ni nanocomposites by atmosphere-controlled sintering and their properties, J. Kor. Ceram. Soc. 39 (2002) 199–203.

[29] S.T. Oh, J.S. Lee, T. Sekino, K. Niihara, Fabrication of Cu dispersed Al_2O_3 nanocomposites using Al_2O_3/CuO and Al_2O_3/Cu-nitrate mixtures, Scripta Mater. 44 (2011) 2117–2120.

[30] T. Ohji, Y.K. Jeoung, Y.H. Choa, K. Niihara, Strengthening and toughening mechanisms of ceramic nanocomposites, J. Am. Ceram. Soc. 81 (1998) 1453–1460.